Journal of the Mechanics and Physics of Solids 111 (2018) 290–307

Contents lists available at ScienceDirect

Journal of the Mechanics and Physics of Solids

journal homepage: www.elsevier.com/locate/jmps

Activity of pyramidal I and II <**c**+**a**> slip in Mg alloys as revealed by texture development

Miroslav Zecevic[a], Irene J. Beyerlein[b], Marko Knezevic[a,*]

[a] Department of Mechanical Engineering, University of New Hampshire, Durham, NH 03824, USA
[b] Mechanical Engineering Department, Materials Department, University of California at Santa Barbara, Santa Barbara, CA 93106, USA

ARTICLE INFO

Article history:
Received 2 September 2017
Revised 1 November 2017
Accepted 8 November 2017
Available online 10 November 2017

Keywords:
Pyramidal slip
A. Dislocations
A. Microstructures
B. Crystal plasticity
B. Polycrystalline material

ABSTRACT

Due to the geometry of the hexagonal close-packed (HCP) lattice, there are two types of pyramidal <**c**+**a**> slip modes: $\{10\bar{1}1\}\langle 11\bar{2}\bar{3}\rangle$ or type I and $\{\bar{1}\bar{1}22\}\langle 11\bar{2}3\rangle$ or type II in HCP crystalline materials. Here we use crystal plasticity to examine the importance of crystallographic slip by pyramidal <**c**+**a**> type I and type II on texture evolution. The study is applied to an Mg-4%Li alloy. An elastic-plastic polycrystal model is employed to elucidate the reorientation tendencies of these two slip modes in rolling of a textured polycrystal. Comparisons with experimental texture measurements indicate that both pyramidal I and II type slip were active during rolling deformation, with pyramidal I being the dominant mode. A single-slip-mode analysis is used to identify the orientations that prefer pyramidal I vs. II type slip when acting alone in a crystal. The analysis applies not only to Mg-4%Li, but identifies the key texture components in HCP crystals that would help distinguish the activity of pyramidal <**c**+**a**> I from pyramidal <**c**+**a**> II slip in rolling deformation.

1. Introduction

Plastic deformation of Mg alloys relies predominantly on the contributions of slip on several independently oriented planes that lead to accommodation of both <**c**> and <**a**> axis deformation. The possible modes of slip are basal <**a**>, prismatic <**a**>, pyramidal <**a**>, and pyramidal <**c**+**a**> slip (Partridge, 1967; Yoo, 1981). In addition to slip, most of Mg alloys deform plastically by deformation twinning modes of which the extension twinning mode $\{10\bar{1}2\}\langle\bar{1}011\rangle$ predominates (Reed-Hill and Robertson, 1957). The study here focuses on the pyramidal <**c**+**a**> slip. From the hexagonal close-packed (HCP) lattice, two types of pyramidal slip modes have been identified: $\{10\bar{1}1\}\langle 11\bar{2}\bar{3}\rangle$ type I and $\{\bar{1}\bar{1}22\}\langle 11\bar{2}3\rangle$ type II. Post-mortem transmission electron microscopy (TEM) characterization or slip trace analyses of deformed Mg specimens have provided evidence of <**c**> and <**c**+**a**> dislocations lying on $\{\bar{1}\bar{1}22\}$ glide planes, suggesting pyramidal type II glide had taken place (Ando and Tonda, 2000; Byer et al., 2010; Obara et al., 1973; Syed et al., 2012; Tonda and Ando, 2002). Direct observations have been reported of moving pyramidal type II dislocations in single Mg crystals of nanoscale dimensions (<100 nm) (Yu et al., 2013). More recent studies on slip traces in deformed pure Mg single crystals have found evidence of both pyramidal I and II slip planes but concluded that pyramidal I slip was the more dominant one (Xie et al., 2016).

Atomic-scale simulations on pure Mg have been carried out to either calculate the generalized stacking fault energy (GSFE) curve for shear along the type I and type II planes, to simulate the dissociation of each type of dislocation to determine its low energy configuration, or to simulate the nucleation of the pyramidal slip dislocation under stress. GSFE

* Corresponding author.
E-mail address: marko.knezevic@unh.edu (M. Knezevic).

https://doi.org/10.1016/j.jmps.2017.11.004
0022-5096/

curves calculated using the Liu or Sun embedded atom method (EAM) potential and density functional theory (DFT) in (Nogaret et al., 2010) predict that the peak in the GSFE curve, related to its formation energy, is higher for pyramidal II than that for pyramidal I. Recent molecular dynamics (MD) simulations using a modified embedded-atom method (MEAM) potential have also been performed to compare the core configurations and self-energies of these two dislocations. For pure Mg, it was found that the core energy of edge pyramidal I dislocations is lower than that of the edge pyramidal II dislocation; however, the opposite was true for their screw dislocations (Wu et al., 2015). MD simulations of direct nucleation under deformation showed formation of pyramidal type I (Li and Ma, 2009), while others have reported nucleation of both types (Kim et al., 2011). DFT calculated GSFE curves suggest that the ideal shear stress for pyramidal I slip would be 10-12 % lower than that for pyramidal II slip (Kumar et al., 2017). Low temperature MD simulations of edge and mixed dislocations found that the low energy state of these dislocations is extended into two equal length partials (Kumar et al., 2017). The pyramidal II configuration is glissile, but that for pyramidal I is not since dislocation core spreads on alternating {3032} and {3034} planes. Recent simulations have also reported that under higher temperatures (>500 K), the dissociated cores of the pyramidal type I and II slip dislocations can reduce their energy by rearranging out of their glide plane. While both are sessile, the reconstructed core for the pyramidal I <**c**+**a**> dislocation type achieved the lower energy state, suggesting it would be less likely to glide (Wu and Curtin, 2015; Wu and Curtin, 2016). Taken altogether, it is clear that local microscopy measurements and atomic scale simulations have been inconclusive.

Atomic-scale simulations and TEM and high-resolution (HR) TEM analyses treat local phenomena but have the advantage of being a direct measurement or observation of an elementary process. Nonetheless, via these methods, it is not possible to assess the dominant deformation mechanism in deformed laboratory samples. A more global gauge of active deformation mechanisms would be the evolution of texture with deformation. In an actual HCP polycrystal with a dispersion of grain orientations, not all grains will activate pyramidal <**c**+**a**> slip and for those grains that do, pyramidal <**c**+**a**> slip is likely not to operate alone. Other slip systems, modes, and mechanisms, such as twinning will be activated alongside pyramidal slip in order to accommodate the deformation of a given grain within the polycrystal. Accordingly, the reorientation tendencies of a grain will be determined by the relative activities of multiple slip and/or twinning modes acting simultaneously. Activation of different slip systems and modes leads to pronounced signatures in texture development. These signs, however, are indirect indicators and relating them to the averaged activation of slip systems often requires interpretation made by a polycrystal model. Over the years, many joint modeling-experimental studies have shown that the development of texture in Mg and Mg alloys highly depends on the initial texture, deformation path, strain rate, and temperature (Ardeljan et al., 2017; Ardeljan et al., 2016a; Chelladurai et al., 2017; Jahedi et al., 2017; Jiang et al., 2007; Kabirian et al., 2015). Texture evolution is sensitive to the relative amounts of slip and twinning modes (Ardeljan et al., 2014; Jain and Agnew, 2007; Knezevic et al., 2013a; Knezevic et al., 2014a; Knezevic et al., 2013b; Knezevic et al., 2012; Knezevic et al., 2016b; Knezevic et al., 2013c; Knezevic et al., 2010). To the authors' knowledge, texture analyses, however, have not been carried out to determine based on texture development whether pyramidal I type or pyramidal II type slip was active.

Polycrystal plasticity models including Taylor (Fromm et al., 2009; Kalidindi et al., 2006; Knezevic et al., 2009; Knezevic et al., 2008a; Knezevic et al., 2008b; Shaffer et al., 2010; Taylor, 1938), self-consistent (Knezevic et al., 2016c; Lebensohn and Tomé, 1993; Lebensohn et al., 2016; Turner and Tomé, 1994; Zecevic et al., 2017b), and finite element (Ardeljan et al., 2016a; Ardeljan et al., 2015; Ardeljan et al., 2016b; Kalidindi et al., 1992; Knezevic et al., 2016a; Knezevic et al., 2014b; Knezevic et al., 2014c; Savage et al., 2017; Zecevic et al., 2016b; Zecevic et al., 2015b, c) based homogenizations have been developed over the past several decades to make the link between the deformation of individual crystals with the deformation of the polycrystal. Crystal plasticity theory is used in most of these models to relate the activity of a set of slip systems with single crystal deformation. Consequently, polycrystal calculations rely heavily on experimental evidence to indicate which of the two types of pyramidal slip modes should be made available. Often times, in modeling Mg and its alloys, one or the other type of pyramidal slip mode is assumed *a priori.* The deformation simulations, particularly for polycrystals, find that many slip and twinning systems operate simultaneously over the period of straining. Since so many deformation modes are active at once, it is difficult to discern which ones are responsible for a particular component or components in the deformation texture.

In this work, we use an elasto-plastic self-consistent (EPSC) model (Turner and Tomé, 1994) to study and interpret the texture evolution in Mg alloys. The model was recently used to simulate texture evolution in the Mg-4%Li under rolling (Lentz et al., 2015a; Lentz et al., 2015b; Risse et al., 2016). This data and material parameters are used in this work. Either pyramidal I or II or a mix of pyramidal I and II slip will be allowed in these calculations, from which we will predict texture evolution and slip and twin activity. It was shown in (Agnew et al., 2001) that alloying magnesium with lithium or yttrium increases the activity of pyramidal <**c**+**a**> slip, hence the Mg-4%Li alloy would appear to be well suited for this study. Deformation textures are a result of the deformation state and here we study texture evolution arising from two distinct deformation states: uniaxial tension/compression and plane strain compression. These polycrystal calculations permit every grain to deform by potentially twinning, basal, prismatic systems, not just pyramidal I or II slip alone. The reorientation trends of pyramidal I and II, when they are acting in isolation, are analyzed using the Single-Slip-Mode (SSM) model "option" within the visco-plastic self-consistent (VPSC) model (Lebensohn and Tomé, 1993).

In what follows, we first investigate the effects of pyramidal I and pyramidal II slip in a realistic setting using the multiscale EPSC model with a thermally activated dislocation density hardening law, in which multiple slip systems, including basal and prismatic must also be activated alongside pyramidal <**c**+**a**> slip. To theoretically study the effects of each slip mode in isolation, we employ a SSM calculation, which permits single crystal deformation to be accommodated by only

Table 1
Model parameters for the evolution of slip and twin mode resistance. The constant for the initial slip resistance enter the following equation $\tau_0 = \frac{A}{1+\exp(B(T-C))}$ and the constants for drag stress enter the following equation $D_0 = E + F\exp GT$. We refer to (Zecevic et al., 2015a) for details of the model; however, we note that some of the parameters have been adjusted from those reported there. T is temperature in kelvin [K].

		<**a**> prism	<**a**> basal	<**c**+**a**> pyr I		<**c**+**a**> pyr II	
				Case 1	Case 3	Case 2	Case 3
τ_0(MPa)	A	2.39×10	1.16	1.21×10^2	1.21×10^2	1.23×10^2	1.36×10^2
	B	3.84×10^{-2}	2.09×10^{-2}	2.19×10^{-2}	2.15×10^{-2}	2.37×10^{-2}	2.15×10^{-2}
	C	4.27×10^2	3.81×10^2	3.57×10^2	3.57×10^2	3.56×10^2	3.57×10^2
$k_1(\mathrm{m}^{-1})$	8×10^8	8×10^7	7.5×10^7	7.5×10^7	7.5×10^7	7.5×10^7	7.5×10^7
D_0(MPa)	E	3.2×10^3	1.5×10^3	3.3×10^3	3.3×10^3	3.3×10^3	3.3×10^3
	F	2.18×10^9	0.0	0.0	0.0	0.0	0.0
	G	-3.68×10^{-2}	1.0	1.0	1.0	1.0	1.0
g	–	3.3×10^{-3}	2.0×10^{-3}	2.0×10^{-3}	2.0×10^{-3}	2.0×10^{-3}	2.0×10^{-3}
$\dot{\varepsilon}_0(\mathrm{s}^{-1})$		10^7	10^7	10^7	10^7	10^7	10^7
$\rho_0(\mathrm{m}^{-2})$		1.5×10^{12}	1.5×10^{12}	1.5×10^{12}	1.5×10^{12}	1.5×10^{12}	1.5×10^{12}
χ		0.9	0.9	0.9	0.9	0.9	0.9
HP (Hall-Petch-like constant)		0	0	0	0	0	0
Latent hardening from slip to TTW		50	50	450	450	450	450
	TTW						
FIF (Finite initial fraction) (Clausen et al., 2008)	0.015						
τ_0(MPa)	25.0						
b(m)	5.54×10^{-11}						
PTS (Predominant twin system)	0.05						
HP (Hall-Petch-like constant)	0.0						

one slip plane. This part of the study is independent of the material properties or hardening model used to activate slip. Together, we demonstrate that texture evolution in rolling can be used to identify pyramidal I or II slip activity in certain orientations of HCP single crystals or in certain preferred textures of HCP polycrystals. For the Mg-4%Li alloy here, it is likely that both pyramidal I and II slip were active with stronger activity of pyramidal I.

2. Modeling framework

2.1. Elasto-plastic self-consistent model for Mg-4%Li

Texture evolution calculations were performed using a mean-field polycrystal code called elasto-plastic self-consistent (EPSC) (Turner and Tomé, 1994). In prior work, a multiscale EPSC model with a thermally activated dislocation density (DD) based hardening law for slip was applied for Mg-4%Li (Lentz et al., 2015a; Risse et al., 2016). The general framework of this model had been developed previously (Zecevic et al., 2017a, 2015a, 2016c; Zecevic and Knezevic, 2015); however, the main adjustment made entailed characterizing the material parameters associated with the DD hardening law for each slip mode and associated with the twinning model for the $\{10\bar{1}2\}\langle\bar{1}011\rangle$ extension twin mode for Mg-4%Li. For this alloy, the prior work made available the following slip modes: basal, prismatic, and pyramidal II <**c**+**a**> slip. The DD hardening law parameters for each mode are a friction stress (τ_0), a drag stress (D_0), activation enthalpy (g), and a trapping rate coefficient (k_1). The friction stress and drag stress are functions of temperature given by: $\tau_0 = \frac{A}{1+\exp(B(T-C))}$ and $D_0 = E + F\exp(GT)$. With a single set of these parameters, the model could reproduce uniaxial tension and compression tests in two distinct loading directions at four different temperatures, from room temperature to 473 K. These parameters are given in Table 1. We designate the simulations performed using basal, prismatic, pyramidal II <**c**+**a**> slip systems and twinning systems "Case 2".

For comparison, we considered a new case ("Case 1"), in which we repeat the EPSC simulations for grains that deform by basal, prismatic, and pyramidal I <**c**+**a**> slip and twinning systems. For this case, the hardening law parameters for pyramidal <**c**+**a**> I need to be characterized. Considering the similarity between pyramidal I and II slip, small adjustments of the parameters associated with pyramidal II slip should suffice. To this end, we assumed that only the initial slip resistance (friction stress) for pyramidal <**c**+**a**> I slip differed from that of pyramidal <**c**+**a**> II slip, while the remaining parameters, governing dislocation-dislocation interactions (drag stress, activation enthalpy, and a trapping rate coefficient) were the same. All material parameters for basal and prismatic slip did not change.

As a third case ("Case 3"), we model the situation in which both pyramidal I and II slip modes are available. Previous experimental analysis has suggested that at 77 K and room temperature, screw <**c**+**a**> dislocations can cross-slip to and from the pyramidal I and II planes (Ando and Tonda, 2000). Observations of this cross-slip process have also been predicted in MD simulation (Ando et al., 2002; Tang and El-Awady, 2014). Although cross-slip and similar discrete dislocation maneuvers cannot be modeled explicitly in EPSC, we can represent the effect by allowing for slip on both pyramidal I and II planes.

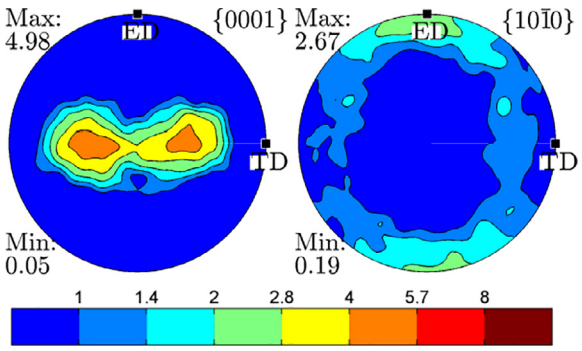

Fig. 1. Basal and prismatic pole figures of the initial texture of the extruded Mg-4%Li material used here measured by x-ray diffraction. Extrusion and transverse direction are denoted as ED and TD repsectivley.

In doing so, we are, however, left with providing *a priori* a CRSS ratio for the initial slip resistance of pyramidal II slip to pyramidal I slip. Recent work on pure Mg single crystals reports evidence by a slip trace analysis of both pyramidal <**c**+**a**> types and a preference of type I over II slip (Xie et al., 2016). They find that the CRSS is 54 MPa for pyramidal I slip. In the same crystal, the Schmid factor for the most preferred pyramidal II slip system was 10% higher. Since it apparently does not activate, the CRSS ratio of type II to type I would at minimum be 1.1. Recent DFT calculations of generalized stacking fault energy (GSFE) surfaces find that the peak energy barrier is 225 mJ/m^2 for the type I pyramidal slip and 250 mJ/m^2 for type II, giving a ratio of 1.11, consistent with the previously mentioned measurement (Kumar et al., 2017). The maximum derviative on this GSFE surface 1/b dE/du can be used as a measure of the ideal shear strength and is 2.36 GPa for pyramidal I slip and 2.65 GPa for pyramidal II slip, giving a ratio of 1.12 (Kumar et al., 2017). Both calculations suggest that it is easier for the pyramidal I dislocation to glide compared to pyramidal II. On this basis, for the third case, with mixed pyramidal I/II slip, we assume that the initial CRSS values for pyramidal II and I bear a ratio of 1.12. The values are given in Table 1.

2.2. Single-slip-mode (SSM) model

In order to study the reorientation tendencies inherent to particular slip mode and applied boundary conditions we use the Single-Slip-Mode (SSM) model "option" within another self-consistent model called visco-plastic self-consistent (VPSC) (Lebensohn and Tomé, 1993). The SSM model enforces the same stress in every crystal while allowing the strain to vary from crystal to crystal (Sachs, 1929). One of the capabilities of the VPSC model is to set the linearization procedures and interaction scheme such that polycrystal compliance corresponds to volume average of grain compliances implying a constant stress over the polycrystal (Lebensohn and Tomé, 1993). We gain the benefit of maintaining the uniform stress tensor across crystals, while permitting strain-rate boundary conditions to be prescribed (Zecevic et al., 2016a). Because of the uniform stress, it is possible for a single slip mode to accommodate the entire strain rate of a given grain, unlike in the self-consistent or Taylor homogenization.

The exact procedure of the proposed SSM analysis is as follows. Each grain is allowed to deform by one mode via a set of slip systems within the particular slip mode under consideration (e.g. twelve slip systems of the pyramidal I slip mode). In other words, multi-slip is allowed but only by slip systems belonging to the active slip mode of interest. Next a constant stress state over the polycrystal (unknown a priori) is iteratively enforced over the grains, under the additional constraint that average strain rate over the polycrystal has to be equal to the applied strain rate (e.g., plane-strain compression strain rate). Only the orientations that have a sufficiently high Schmid factor on the allowed slip systems for a given uniform stress will activate and strain rate will vary from grain to grain. The main difference between the single slip mode analysis employed here and Schmid factor analysis is the additional constraint imposed on the average strain rate over the polycrystal, which in turn defines the uniform stress tensor in the case of applied mixed or strain rate boundary conditions. Next, the resulting grain reorientation can be calculated using the shear rates of all the slip systems within the slip mode under consideration. Therefore, if for a given stress state a particular grain is oriented poorly for slip on slip systems of the slip mode under consideration the resulting shear rates will be zero, the grain will not deform and hence the reorientation will be zero.

3. Results and discussion

The material studied here started as a processed Mg-4%Li, which was extruded with an extrusion ratio of 61:1 at a processing temperature of 573 K and not annealed afterwards (Risse et al., 2017). For this study, uniaxial tension and plane-strain compression of the extruded Mg-4%Li were simulated and predictions for the stress-strain response and deformation textures are compared with experiments. Unless stated otherwise, we used the EPSC model and in a few instances calculations were repeated using the proposed SSM analysis to isolate orientations that are best oriented for a particular slip mode

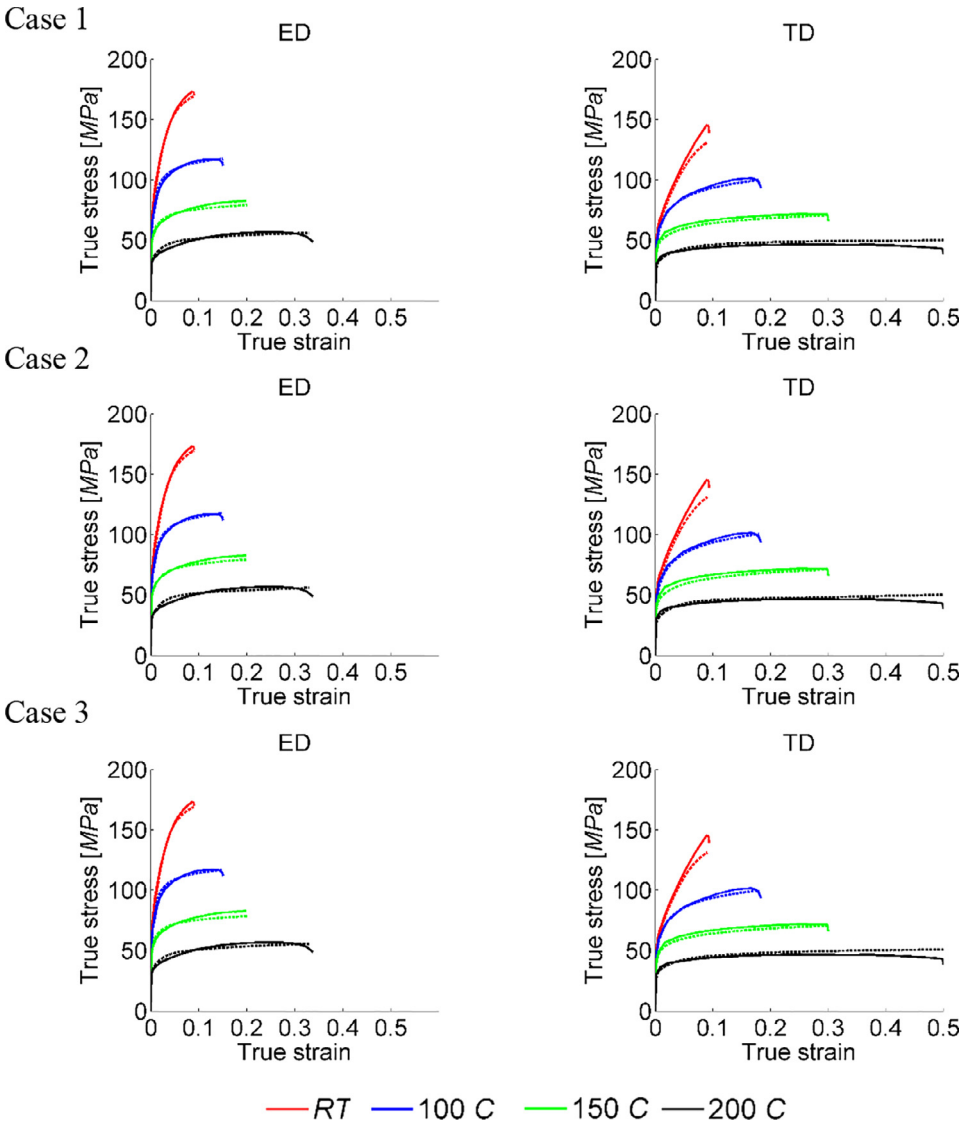

Fig. 2. Comparison of measured (solid lines) and calculated (dashed lines) tensile true stress-true strain curves in extrusion and transverse directions (ED and TD) for Mg-4%Li at room temperature (RT), 100 °C, 150 °C and 200 °C for three cases considered. We see that all three sets of slip modes (basal, prismatic, pyramidal I, and extension twinning), (basal, prismatic, pyramidal II, and extension twinning), and (basal, prismatic, pyramidal I, pyramidal II, and extension twinning) provide good agreement with the measurement.

and to study their reorientation trends. Analysis of the textures but not stress-strain response are used to draw conclusions on the relative activity of the pyramidal I/II modes.

3.1. Uniaxial tension of Mg-4%Li

We first use the EPSC model to simulate uniaxial tension tests under the four temperatures reported in (Risse et al., 2016). Details on the material and experimental mechanical test procedures can be found in (Risse et al., 2016). The material parameters used to obtain the same agreement in the stress-strain curves for all three cases is given in Table 1. While the stress-strain curves are used for characterization of hardening parameters for Case 1 including pyramidal I slip and Case 3 allowing for mixed pyramidal I/II slip, other model outputs, such as texture evolution and slip activity are predictions and thus serve to validate the model and indicate slip activity.

Deformation textures can be sensitive to the initial texture, strain level, temperature, and strain rate. When directly comparing calculated and measured textures, we import the initial texture as measured from x-ray diffraction (XRD), input the actual temperatures and strain rate of the test, and make the comparison for the same deformation strain levels. The

initial texture of the extruded Mg-4%Li material used in these tension tests is presented in the form of basal and prismatic pole figures in Fig. 1. Pole figures in the present work are equal area representations. As shown in the basal pole figure, the material exhibits a preferred texture from the extrusion process used to produce the final sheet form. Two closely separated, diffuse basal peaks along the transverse direction (TD) have formed.

The model represented the initial texture using 2000 orientations and grain shapes that were initially spherical thus neglecting the influence of sporadically observed elongated grains (Risse et al., 2016). As in the experiment, the material was strained in tension in either the extrusion direction (ED) or TD of the extruded sheet at an applied rate of 1.6e-4/s.

Fig. 2 compares model results for Case 1 (pyramidal I), Case 2 (pyramidal II), and Case 3 (pyramidal I/II) with the measured stress-strain curves in ED tension and TD tension at four temperatures. The agreement between the model and measurements is good.

Fig. 3 shows the corresponding relative slip and twinning activity plots at two temperatures: room temperature and 100 °C. The results reveal some pyramidal slip activity in ED tension and practically no pyramidal slip activity in TD tension. In ED tension, because of difference in initial CRSS between pyramidal I and II slip, there is less basal slip activity and more pyramidal $<\mathbf{c}+\mathbf{a}>$ activity in the pyramidal I Case 1 than in the pyramidal II only Case 2. In TD tension, extension $\{10\bar{1}2\}\langle\bar{1}011\rangle$ twinning was favored over pyramidal $<\mathbf{c}+\mathbf{a}>$ slip. We find that in Case 3, with both pyramidal I/II available, both are active but pyramidal I slip dominates.

Fig. 4 compares the deformation texture at the end of uniaxial straining for ED and TD tension for all three cases with the experimental measurement at room temperature and 100 °C. The three cases achieve good agreement with experiment but among them, show negligible differences in the calculated texture evolution. For TD tension this similarity is not surprising since pyramidal $<\mathbf{c}+\mathbf{a}>$ slip was not active, whereas for ED tension, wherein pyramidal $<\mathbf{c}+\mathbf{a}>$ slip contributed a substantial amount, this result suggests that which type of pyramidal $<\mathbf{c}+\mathbf{a}>$ slip does not impact texture evolution in uniaxial straining.

3.2. Rolling of Mg-4%Li plate at room temperature

3.2.1. EPSC predictions for plane-strain compression of Mg-4%Li

Having characterized and validated the model for either pyramidal I or pyramidal II slip in uniaxial deformation, we subsequently employ the model to investigate the differences in lattice reorientation tendencies and texture evolution due to pyramidal I vs. II type slip in plane strain compression (PSC) an idealized representation of the deformation state developed in rolling (Kocks et al., 1998). PSC best applies to the center of the rolled sheet away from the ends and top and bottom surfaces that contact the rolls. The EPSC calculations were performed to predict texture evolution in PSC under Case 1 (with pyramidal I slip), Case 2 (with pyramidal II slip), and Case 3 (with mixed pyramidal I and II slip) and compared with experimental observation as guidance on which type of $<\mathbf{c}+\mathbf{a}>$ slip may dominate in deformation.

For this work, the same Mg-4%Li studied in (Risse et al., 2016) was rolled at room temperature to 54% reduction and the texture was measured using neutron diffraction at the Los Alamos Neutron Science Center (LANSCE) using the HIPPO spectrometer. Prior to rolling, however, the Mg-4%Li material was annealed and consequently, the initial texture was altered from that of Fig. 1. The initial texture for the rolling experiments is provided in Fig. 5. As shown, two widely separated basal peaks along the transverse direction (TD) have formed. A predominant orientation within this peak is denoted with a black dot.

Fig. 6 shows the variation in the relative activity of the various slip modes and twinning during the PSC deformation. In all three cases, basal slip and prismatic slip are active in the beginning of deformation and pyramidal $<\mathbf{c}+\mathbf{a}>$ slip develops later in deformation, and tensile twinning occurs but is not profuse. Beyond roughly 40% rolling strain, pyramidal $<\mathbf{c}+\mathbf{a}>$ slip contributes 30% or more to the deformation. This development occurs because $<\mathbf{c}+\mathbf{a}>$ slip is the harder mode, requiring either reorientation to orientations favoring pyramidal slip and/or hardening of the $<\mathbf{a}>$ slip modes. In Case 3, we see that both pyramidal I/II slip are activated; however, with a CRSS ratio for pyramidal II/pyramidal I of 1.12, pyramidal I slip dominates. As a consequence, bulk texture results for Case 1 and Case 3 are not expected to be different.

The relative activities studied in Fig. 6 provide the values averaged over the entire polycrystal. A more refined analysis is carried out to provide the activities within each grain and its history. Fig. 7 plots the instantaneous reorientation trends due to pyramidal I and II slip for 300 grains with highest reorientation angle, later in the deformation at −0.42 strain of PSC along ND and expansion in RD, when pyramidal slip is sufficiently active in a {0001}, $\{10\bar{1}0\}$ and $\{11\bar{2}0\}$ pole figures. The corresponding reorientation velocities (given in Fig. S1 of the supplementary material) are calculated as vectors, whose length is proportional to the velocity. The vector connects the initial (here the initial texture is at −0.42 strain) to the final orientation (at the end of a given strain increment) of the selected pole and because the strain increment is small, 0.001, the direction of this arrow lied parallel to the reorientation velocity of the pole. Furthermore, the magnitude of the velocity vector is scaled by an arbitrary constant for better illustration purposes. The scaling factors are indicated in the figure captions. Grains showing activity of pyramidal I or II slip may also be simultaneously activating other modes of slip. Therefore, at this point we can only conclude that the results plotted on Figs. 7 and S1 are valid only for that specific state within the polycrystal. If we decreased, for example, the slip resistance of prismatic slip, the grains activating pyramidal modes and their reorientation tendencies could be altered. Fig. 7a shows the reorientation of grains in which pyramidal I slip is active and Fig. 7b are those grains in which pyramidal II slip is active. Generally, more grains activate pyramidal I slip than pyramidal II slip. From the basal pole reorientation velocity map, we observe that grains in which pyramidal II

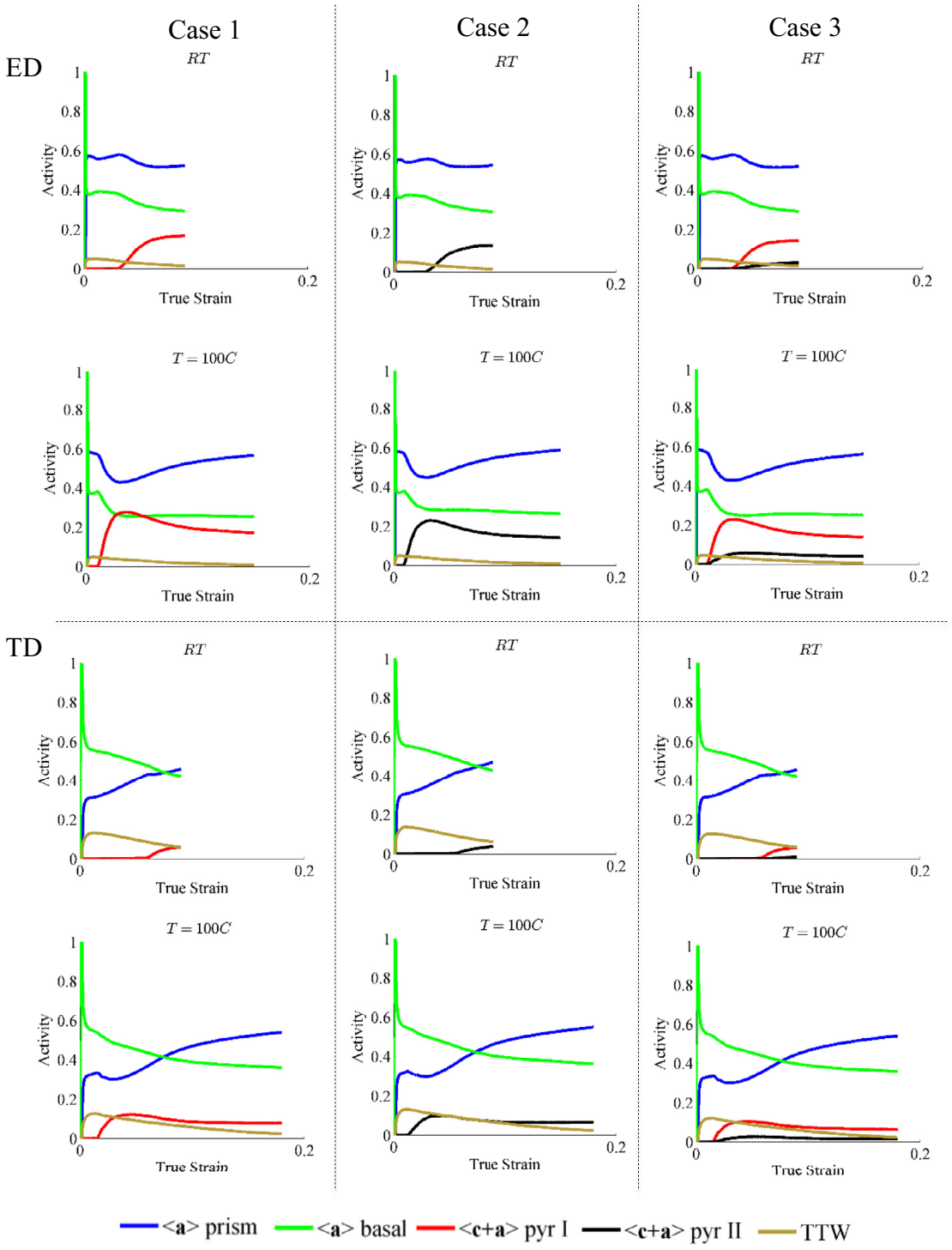

Fig. 3. Simulated relative activity plots in ED and TD tension for extruded Mg-4%Li at room temperature (*RT*) and 100 °C for cases 1, 2, and 3.

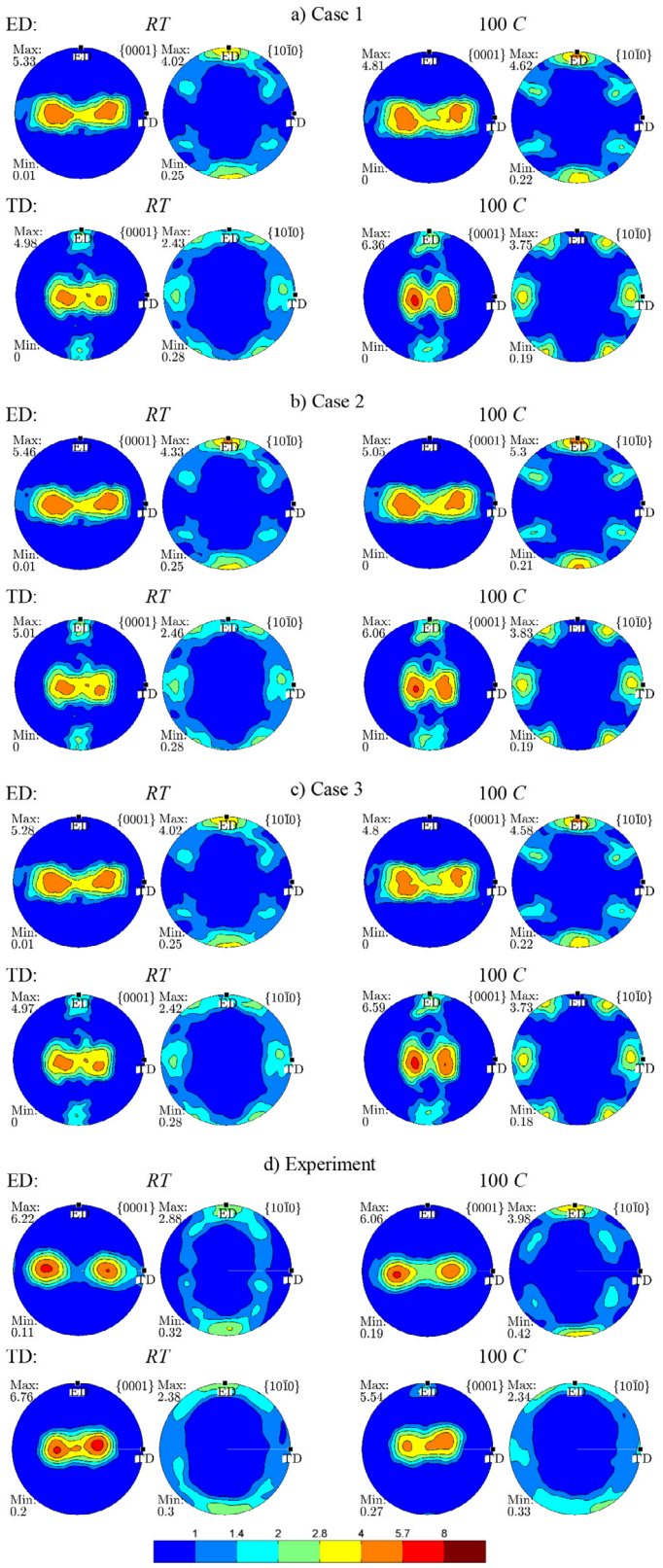

Fig. 4. Comparison of measured and calculated tensile deformation textures for Mg-4%Li at room temperature and 100°C. (a) Case 1: the set of slip modes for basal, prismatic, pyramidal I, (b) case 2: the set of slip modes for basal, prismatic, pyramidal II, (c) case 3: the set of slip modes for basal, prismatic, and both pyramidal I/II and (d) experimental textures measured by XRD.

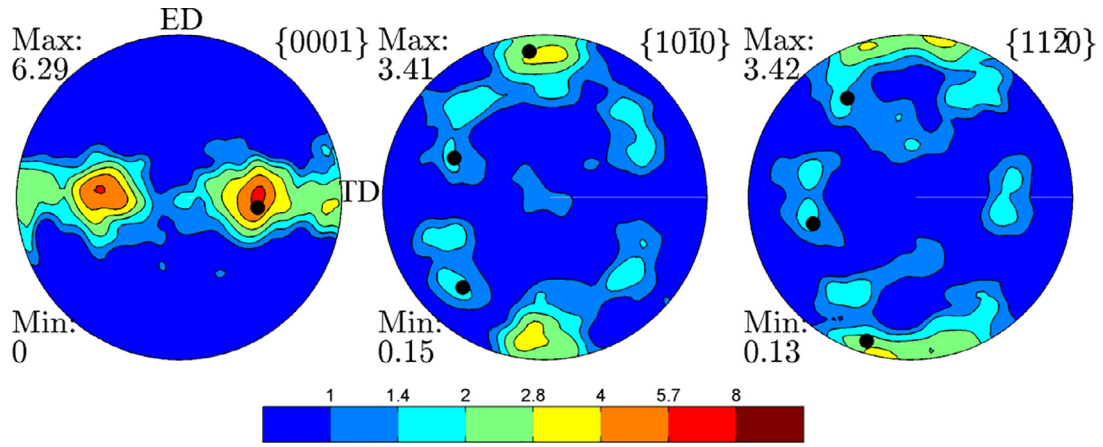

Fig. 5. Pole figures of extruded and annealed Mg-4%Li prior to rolling measured using the HIPPO spectrometer. The black dot corresponds to one of the peak intensity orientations with Bunge Euler angles [83° 40° 47°] when **x**||TD and **y**||ED.

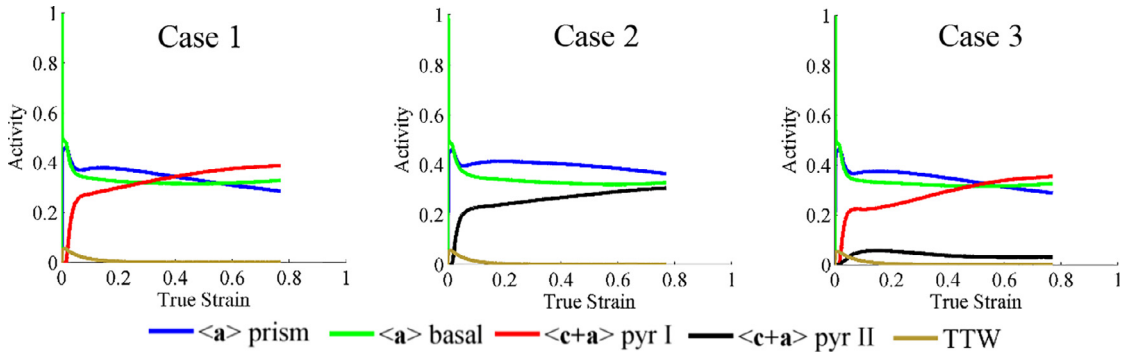

Fig. 6. Simulated relative activity plots for rolling of extruded and annealed Mg-4%Li at room temperature to 54% reduction for cases 1, 2 and 3.

slip is active have their c-axes located approximately axisymmetrically around the ND (Fig. 7b). The grains with the highest activity of pyramidal II slip have their c-axes in the RD-ND plane. In contrast, grains that activate pyramidal I slip have their c-axes oriented symmetrically about the TD as two spread peaks from the ND. It is important to note that it is the activity of pyramidal slip that causes the separation along the RD of the initial TD peaks, which is in agreement with (Agnew et al., 2001). Also we observe a slight tendency for pyramidal II slip to reorient the c-axes in the TD direction. Finally, we note that pyramidal II slip is most active in orientations with {11$\bar{2}$0} poles parallel with RD while {11$\bar{2}$0} poles of the orientations that activate pyramidal I slip are 15–20° away from RD in the RD-TD plane. Results for Case 3 are similar to those for Case 1 and hence are not shown.

Fig. 8 compares the simulated texture evolution in Cases 1, 2, and 3 after 54% reduction with the measured rolling texture. If large enough volume close to the center of the plate was considered, the rolling (orthotropic) symmetry would become apparent. Four-fold rolling symmetry was imposed to the deformation textures in order to remove small variabilities present in both experiment and simulations (Bhattacharyya et al., 2015; Knezevic and Bhattacharyya, 2017). Corresponding textures without symmetry imposed are included in the supplementary material (Fig. S2). In the calculated deformed texture for Case 2, the peak texture components have their c-axes oriented approximately axisymmetrically about the ND in form of six peaks. In Cases 1 and 3 c-axes are oriented symmetrically in the RD from the ND forming four distinct peaks. The basal peaks are too close to the initial TD peaks in Case 2, indicating that pyramidal II activity in the initial TD peaks was not strong enough to reorient them to the peak orientations that are present in the deformation textures of Cases 1 and 3 and experimental results. This is in agreement with the reorientation trends given on Fig. 7 which indicate that initial TD peaks are better oriented for slip on pyramidal I than on pyramidal II. In addition, the tendency of the pyramidal II to reorient the basal poles in the TD direction slowed down movement of the initial TD basal peaks towards RD. However, it should be noted that the peaks along the RD direction, which are characteristic for Case 2, are present in the experimental measurements. This is again in agreement with Fig. 7, which shows that pyramidal II is the most active in the peaks along RD. In the Case 2 we see clustering of the {11$\bar{2}$0} poles along RD while in Cases 1 and 3 we see development of two peaks

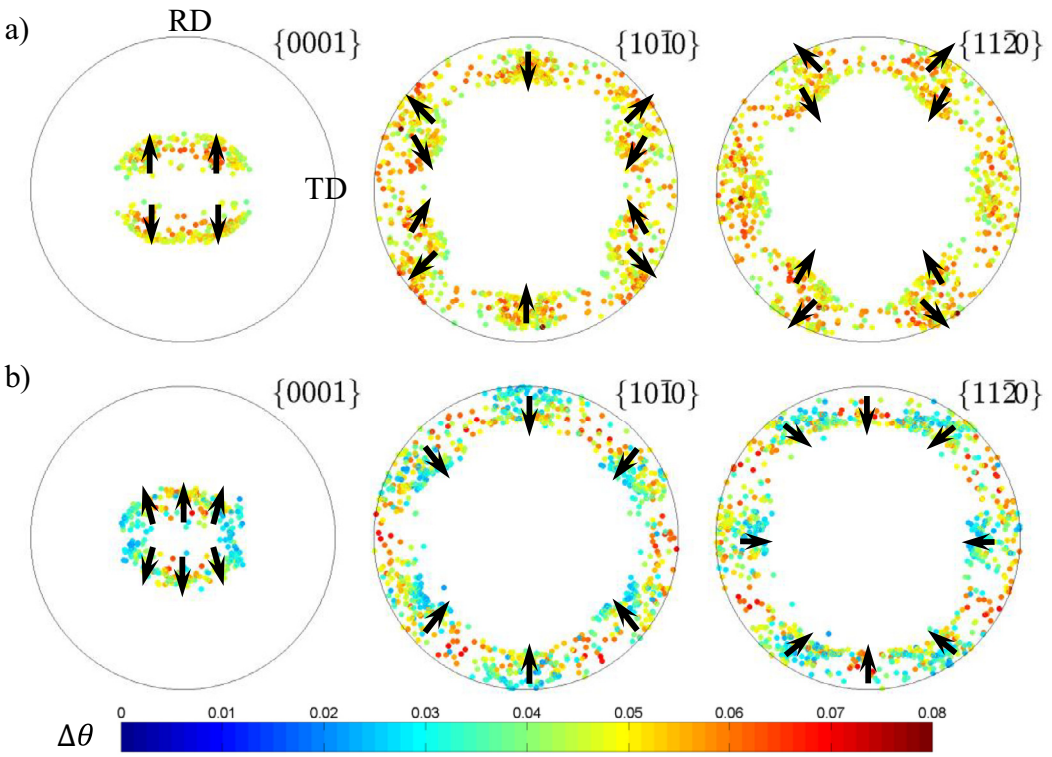

Fig. 7. Reorientation trends for (a) pyramidal I slip and (b) pyramidal II slip from EPSC at −0.42 strain along ND, plotted for 300 grains with highest reorientation and color-coded according to the angle of reorientation (degrees) for strain increment of 0.001. The arrows are superimposed to indicate the overall directions of reorientation. (For interpretation of the references to color in this figure legend, the reader is referred to the web version of this article.)

about 15° away from the RD in the RD-TD plane, which is consistent with the experimental results and reorientation plots on Fig. 7.

Since Case 3 does not allow pyramidal II to activate, we have lowered the initial CRSS of pyramidal II slip to the value of pyramidal I slip and called this "Case 3.1". The uniaxial tension stress-strain curves and deformation textures are practically unaffected. The deformation texture after 54% reduction for Case 3.1 is plotted on Fig. 8 as well. Case 3.1 develops both basal lateral peaks and the basal RD peaks and thus reproduces the experimentally seen features the best.

In order to further corroborate the finding that initial TD peaks are better oriented for slip on pyramidal I slip we track the grain orientation with the highest intensity in the initial texture (marked in Fig. 5). Behavior of this orientation would approximately correspond to average behavior of TD peaks in initial texture. When activities within this orientation for Cases 1 and 2 are compared, it is observed that activity of pyramidal II slip (case 2) is noticeably lower than activity of pyramidal I slip (Case 1).

The results indicate that Case 2 does not predict texture formation under PSC satisfactorily for the calibrated set of parameters. However, pyramidal slip is not the only deformation mode active and thus, considering different ratios of slip and twinning resistances could improve the overall predictions of the Case 2. To this end, we adopt the approach given in (Agnew et al., 2001) for magnesium and magnesium alloys and run a large number of PSC simulations for Case 2, assuming different ratios of the initial slip resistances: basal-prismatic-pyramidal II-extension twinning: 1:(1–12):(1–12):(1–4). The hardening is set to a minimal value for each mode to represent an almost perfectly plastic response. The simulation results indicate that slip resistance ratios approximately in the range of ratios 3:1:7:1 give texture predictions most consistent with the measured texture. This ratio is qualitatively similar to the one adopted in (Risse et al., 2016) and used in this study, while the predicted textures and activities for PSC closely resemble the ones given in Figs. 8 and 6 for Case 2. The results also indicate that higher activity of pyramidal II slip mode (for ratio e.g. 4:1:4:1) results in a larger separation of the initial basal TD peaks along the RD direction, which is seen in the experiment. However, it also causes a shift of the initial basal peaks away from the center in the TD direction resulting in final basal lateral peaks, which are too spread apart in TD direction. In addition, the increase in pyramidal II activity causes strengthening of the {11$\bar{2}$0} peak in the RD direction, which is in

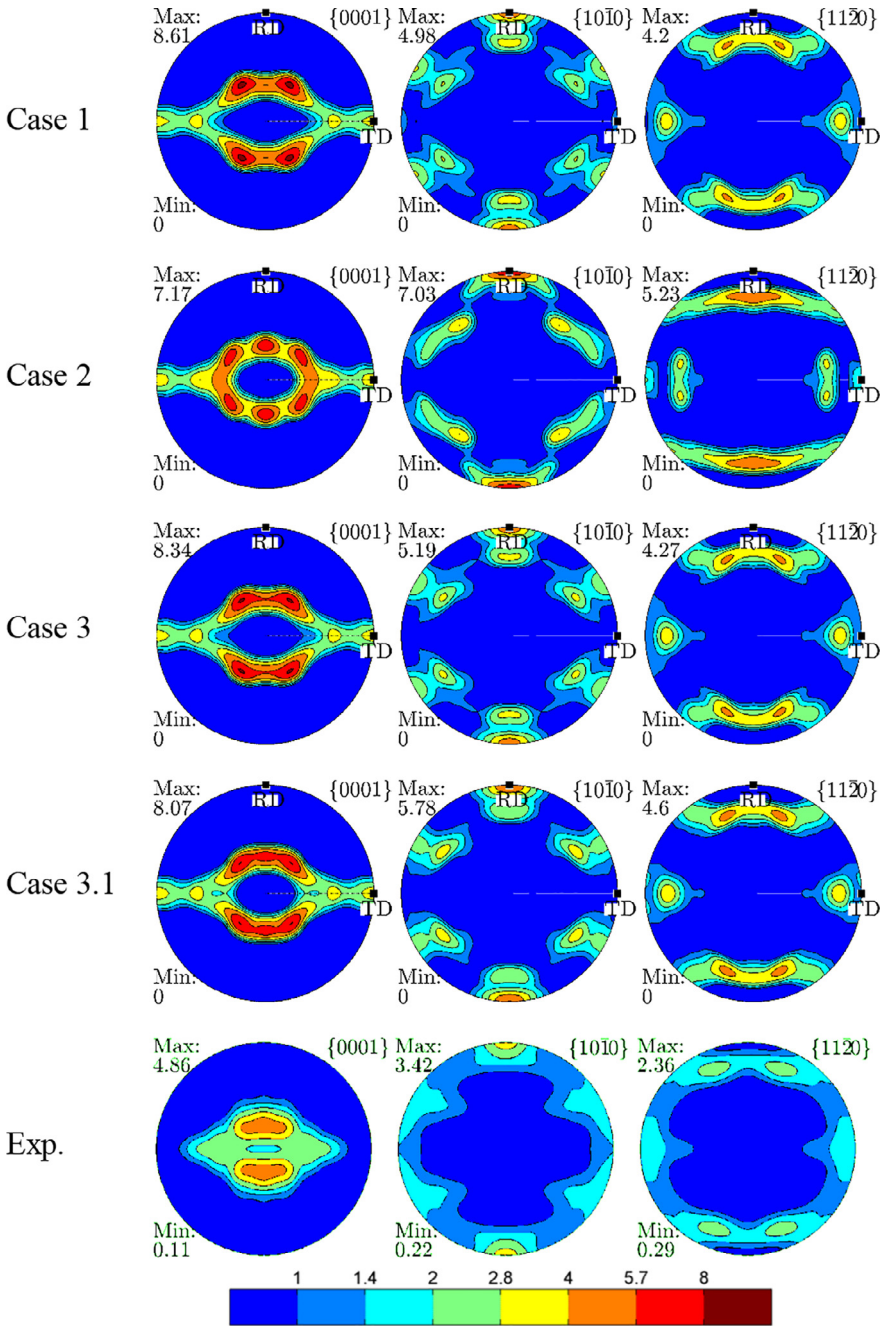

Fig. 8. Comparison of the calculated and measured textures of extruded and annealed Mg-4%Li rolled to 54% reduction at room temperature for cases 1, 2, 3 and 3.1.

contradiction with experimental results. Therefore, it seems that Case 2 is not capable of predicting certain deformation texture features correctly in the case of PSC for any ratio of initial slip resistances.

In conclusion, we found that experimental texture possesses features characteristic of both pyramidal I and II slip modes. Consequently, the predicted deformation texture for Case 3.1 matched the best with the experimental texture while Case 3 predicted results similar to the Case 2. It was also noted that grains of different orientation activate pyramidal I and II which was the main cause of the observed texture differences between different cases. In addition, it was shown that different activities of basal slip, prismatic slip and tensile twinning do not improve the predictions of Case 2 for PSC deformation texture, confirming the hardening parameters reported in (Risse et al., 2016). In the next section we perform a detailed

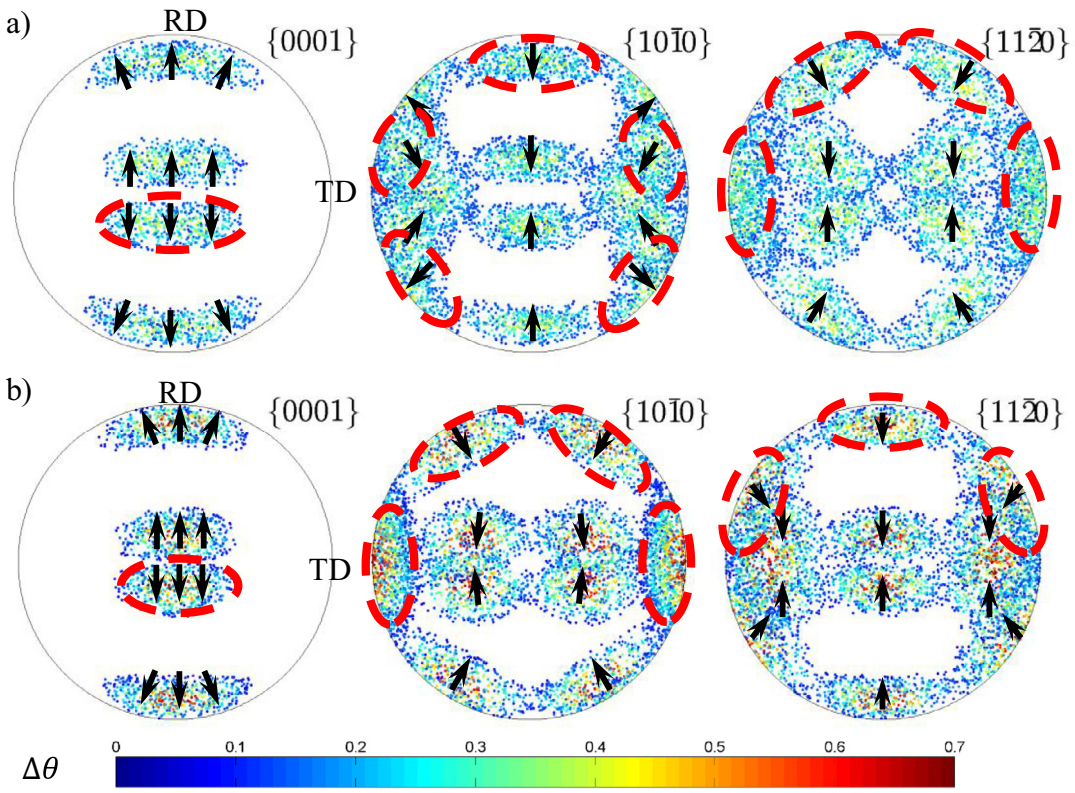

Fig. 9. The reorientation trends for the {0001} and {10$\bar{1}$0} poles in PSC when the (a) pyramidal I slip mode only and (b) pyramidal II slip mode only are available to carry the deformation. Only 2000 most active grains were plotted and color-coded according to angle in degrees of reorientation during one increment in strain of 0.001. The arrows are superimposed to indicate the overall directions of reorientation. RD and TD indicate rolling direction and transverse direction. (For interpretation of the references to color in this figure legend, the reader is referred to the web version of this article.)

analysis of pyramidal I and II slip reorientations in order to understand the influence of texture and other modes on the observed reorientation trends and why some grains favor pyramidal I and others pyramidal II slip.

3.2.2. Reorientation trends during plane-strain compression via the single-slip-mode analysis

Here we employ SSM analysis as a method to isolate the orientations that are best oriented for a particular slip mode and to study their reorientation trends. In these calculations, the main constraint we impose is that only one slip mode is permitted. In this way, it is well suited for the pyramidal <**c**+**a**> slip analysis as single-slip deformation to potentially distinguish between the favorable grains selected and reorientations caused by pyramidal <**c**+**a**> slip types I and II. Crystallographically, pyramidal I and II are different in two ways: first, they act on different crystallographic planes, {10$\bar{1}$1} for type I and {$\bar{1}\bar{1}$22} for type II, and second, the number of Burgers vectors on each plane is two for type I and one for type II, giving 12 slip systems for type I and 6 slip systems for type II. Any number of slip systems per given plane could be selected to accommodate strain rate of a grain in the polycrystal.

We consider a polycrystal containing 10,000 distinctly and randomly oriented grains deformed under plane strain compression. Fig. 9 shows the reorientation angle-color-coded maps on a basal and prismatic pole figures, where the angle of reorientation in degrees (after 0.001 compressive strain along ND) is designated by color. These reorientation trends are calculated when only pyramidal I slip or pyramidal II slip is permitted. In addition, the corresponding reorientation velocities are also calculated. However, due to large number of orientations and thus a large number of arrows we have decided to show only the general trends of reorientation for 2000 most active orientations on Fig. 9. The velocity plots using 1000 grains are presented in the supplementary material (Fig. S3).

Fig. 9a exposes the grain orientations with the highest reorientation magnitude, which are essentially the orientations that activate pyramidal I slip in PSC. The grains with low reorientation magnitude are not oriented well for slip on any of

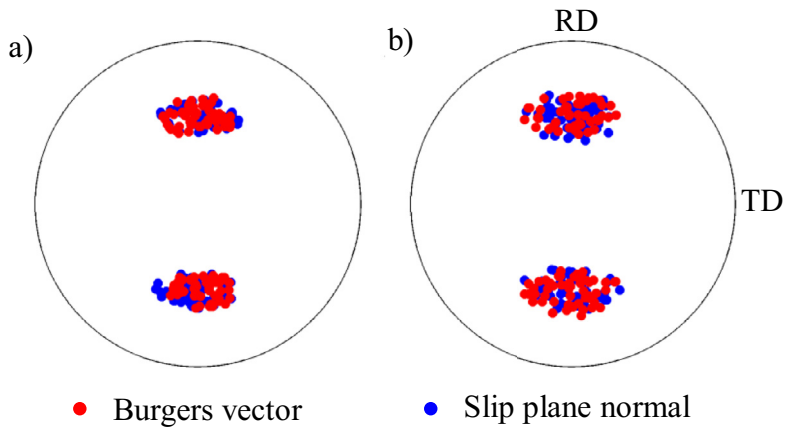

Fig. 10. Equal-area projections of Burgers vector (red) and slip plane normal (blue) of the most active slip system in 100 grains with highest strain rate in PSC, plotted in the sample frame when (a) pyramidal I slip mode only and (b) pyramidal II slip mode only are available for carrying the deformation. (For interpretation of the references to color in this figure legend, the reader is referred to the web version of this article.)

the slip systems of pyramidal I mode under the applied PSC strain rate boundary conditions. The special grain orientations with the largest velocity of basal poles are marked in red. These orientations are special as they are orientations in which pyramidal I slip would be the most active under rolling, according to SSM model. The same reorientation velocity analysis is carried out for pyramidal II slip. Fig. 9b shows the reorientation trends for the basal and prismatic poles for 2000 most active grains color-coded according to reorientation angle, and as before, also contains in red the grains with the highest velocity.

We observe slight differences in the maps for pyramidal I and II slip. The maximum reorientation velocity grains for pyramidal II slip are different from those associated with pyramidal I slip. This is noticeable on the reorientation maps of the $\{10\bar{1}0\}$ and $\{11\bar{2}0\}$ poles. Unlike pyramidal I slip, pyramidal II slip favors formation of two narrow peaks on the basal pole figure. These peaks are denser than those for pyramidal I slip since unlike pyramidal I slip, every pyramidal II slip plane has only one slip direction. Accommodation of the applied strain rate is less flexible and hence fewer grains can activate pyramidal II slip alone. Since a smaller number of grains accommodate the applied strain rate, the grains associated with the pyramidal II slip peak orientations would deform more than the grains corresponding to the pyramidal I slip peak orientations. This is why the reorientation angles of the most active grains are higher in pyramidal II slip than in pyramidal I slip.

One noteworthy result is agreement achieved between the SSM predictions for the grains that activate the pyramidal I or II slip modes and their reorientation trends and the EPSC reorientation results (Fig. 7). The former SSM analysis is based only on the geometry of slip mode under consideration and applied boundary conditions, while the self-consistent simulations allow for active multiple slip modes and different slip resistances within each grain. Similar trends for textured polycrystals between these two analyses imply that the observed trends in reorientation tendencies for one slip mode are not significantly influenced by the other modes or the texture. As further verification, we compared the SSM analysis results with self-consistent results for different strain levels and initial slip resistance ratios, achieving similar agreement each time. Evidently the observed reorientation trends and which orientations activate a given slip mode seem to be inherent to the given slip mode and applied boundary conditions. An exception arises in self-consistent simulations when one slip mode has considerably lower resistance than that of the other modes, since this easy mode will tend to activate in majority of grains. As further support, we note that the locations of these most active pyramidal <**c**+**a**> slip orientations are very similar to the split basal peak texture that develops in the stable rolled textures of some Mg alloys or other HCP metals (Wang and Huang, 2003).

By analyzing the activities within grains with highest strain rate in the SSM results, we found that, in the case of pyramidal II slip, only one slip system was active. The Burgers vector and slip plane normal of active slip system lay in the RD-ND plane and were tilted 45° from the ND (as shown in Fig. 10b). This implies that in these orientations the symmetric Schmid tensor of the active slip system is essentially parallel to the applied strain rate. Consequently, the strain rate within these grains is equal to the applied one. A list of all the orientations in which symmetric Schmid tensor of at least one slip system is exactly parallel to applied PSC strain rate for pyramidal I or II is given in the appendix (Table A1). Pole figures of these orientations are also provided (Fig. A1 in appendix). In the case of pyramidal I slip, the grains with highest strain rate had either one or two slip systems active. The Burgers vector and slip plane normal of most active slip system within grains with highest strain rate are shown in Fig. 10a. The activation of two slip systems can occur because there are two Burgers vectors per slip plane in pyramidal I slip, allowing for the strain rate to be jointly accommodated by shear in both Burgers vector directions.

The fact that grains activating pyramidal I or II slip in SSM and EPSC results match well indicates that a particular slip mode is most active within those orientations in which it can accommodate the largest portion of the applied strain rate. Within these orientations the symmetric Schmid tensor of the most active system will be almost parallel to the applied PSC strain rate. Due to geometrical differences between the pyramidal I and II slip systems, they will activate in different orientations, resulting in a different texture evolution observed in PSC simulations.

3.3. Plane-strain compression to high reductions

When Mg-4%Li sheet is rolled to higher reductions, the texture tends to develop two concentrated basal peaks in the RD direction characteristic for Mg alloys (Agnew et al., 2001; Li et al., 2011; Styczynski et al., 2004). The question to ask then is would both pyramidal I and II slip predict the same stable texture components? To address it, rolling of Mg alloy to 90% reduction at 400 C is simulated and compared to results reported in (Li et al., 2011). For this calculation, we use the visco-plastic self-consistent model with grain fragmentation scheme in order to more accurately represent the evolution of grain shape and thus the reorientation due to local grain spin (Beyerlein et al., 2003; Tomé et al., 2002). We have again considered three cases making available basal and prismatic slip and either pyramidal I (Case 1), pyramidal II (Case 2) or mixed pyramidal I/II slip (Case 3). We have tested multiple ratios of slip resistances close to the ones found in (Styczynski et al., 2004) but we report results for only one representative ratio for which all the cases give reasonable predictions (Fig. A2 in appendix): basal-prismatic-pyramidal: 1-1.5-2.5. The results indicate that at intermediate and high reductions, pyramidal II predictions display weaker RD basal peaks with a greater spread along the TD direction. Reorientation due to the pyramidal II slip mode causes the RD peaks to spread in the TD direction, while the pyramidal I slip reorientation causes strengthening of the RD peaks. Consequently, simulations using pyramidal I slip agree better with the measurements reported in (Li et al., 2011).

6. Conclusions

In this work, we use polycrystal plasticity calculation to investigate the effect of pyramidal I and II slip in the evolution of texture during uniaxial and rolling deformation of an Mg alloy, Mg-4%Li. Simulations were performed using an EPSC polycrystal model, which allows for the plastic deformation proportion for each grain to be accommodated by multiple slip modes. In addition, we carried out lattice reorientation velocity calculations using the SSM model in order to enforce accommodation of an applied deformation with only one active slip mode in all grains. The EPSC analyses for the texture evolution of a polycrystal of Mg-4%Li in rolling indicate that both pyramidal I and II accommodated <**c**> axis deformation with pyramidal I being the dominant mode. Deformation texture evolution showed signatures of pyramidal I slip since the high intensity peaks in the initial texture were oriented better for pyramidal I slip than pyramidal II slip. In addition, pyramidal I slip was active over a wider range of grains, as a result of the crystallography of the pyramidal I slip systems. However, we also noted signatures of pyramidal II slip in the experimental results indicating that pyramidal II slip is activated within grain orientations, where it is more favorable than pyramidal I slip. Analysis of PSC texture predictions for large number of slip and twinning resistance ratios indicates that pyramidal II slip alone is not capable of reproducing certain experimental texture features regardless of the relative activity of other deformation modes. Based on these results, we recommend a *bulk* method to assess which pyramidal <**c**+**a**> slip mode dominates based on plane strain compression of single crystals or strongly textured polycrystals oriented such that the Schmid tensors of either pyramidal I or II slip systems are parallel to the applied strain rate.

Acknowledgments

This work is based upon project supported by the US National Science Foundation (NSF) under grant No. CMMI-1650641. The authors gratefully acknowledge this support. I.J.B. acknowledges financial support from NSF under grant No. CMMI-1728224. I.J.B. would like to acknowledge travel support to UNH through the STEM Women Visiting Scholars Program at the University of New Hampshire funded by NSF grant No. 1209189.

Appendix

Figs. A1 and A2, Table A1.

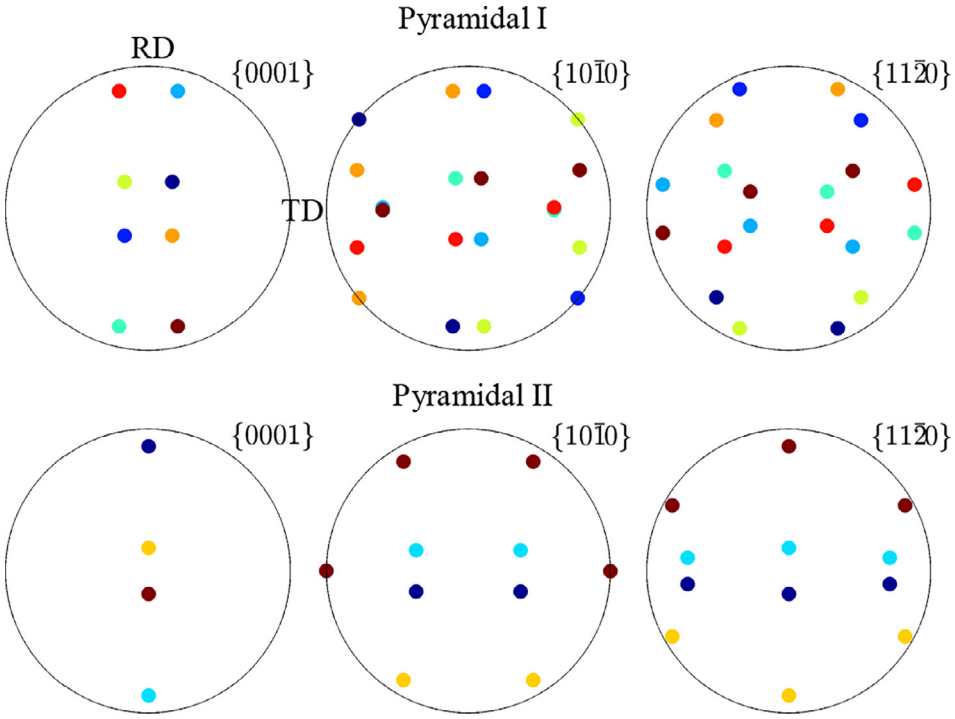

Fig. A1. Pole figures of orientations with symmetric Schmid tensor of at least one slip system exactly parallel to applied PSC strain rate for pyramidal I and II slip corresponding to Table 1.

Table A1
Orientations with symmetric Schmid tensor of at least one slip system exactly parallel to applied PSC strain rate for pyramidal I and II slip. Euler angles are indicated relative to the (RD || **x**, ND || **z**) sample frame.

Bunge–Euler angles of the orientations with symmetric Schmid tensor of at least one slip system parallel to the applied PSC strain rate					
Pyramidal I			Pyramidal II		
φ_1	Φ	φ_2	φ_1	Φ	φ_2
48.8	20.7	31.9	90.0	76.8	30.0
228.8	20.7	31.9	270.0	76.8	30
76.1	74.6	11.2	90.0	13.2	30.0
256.1	74.6	11.2	270.0	13.2	30.0
131.2	20.7	28.1			
311.2	20.7	28.1			
103.9	74.6	48.8			
283.9	74.6	48.8			

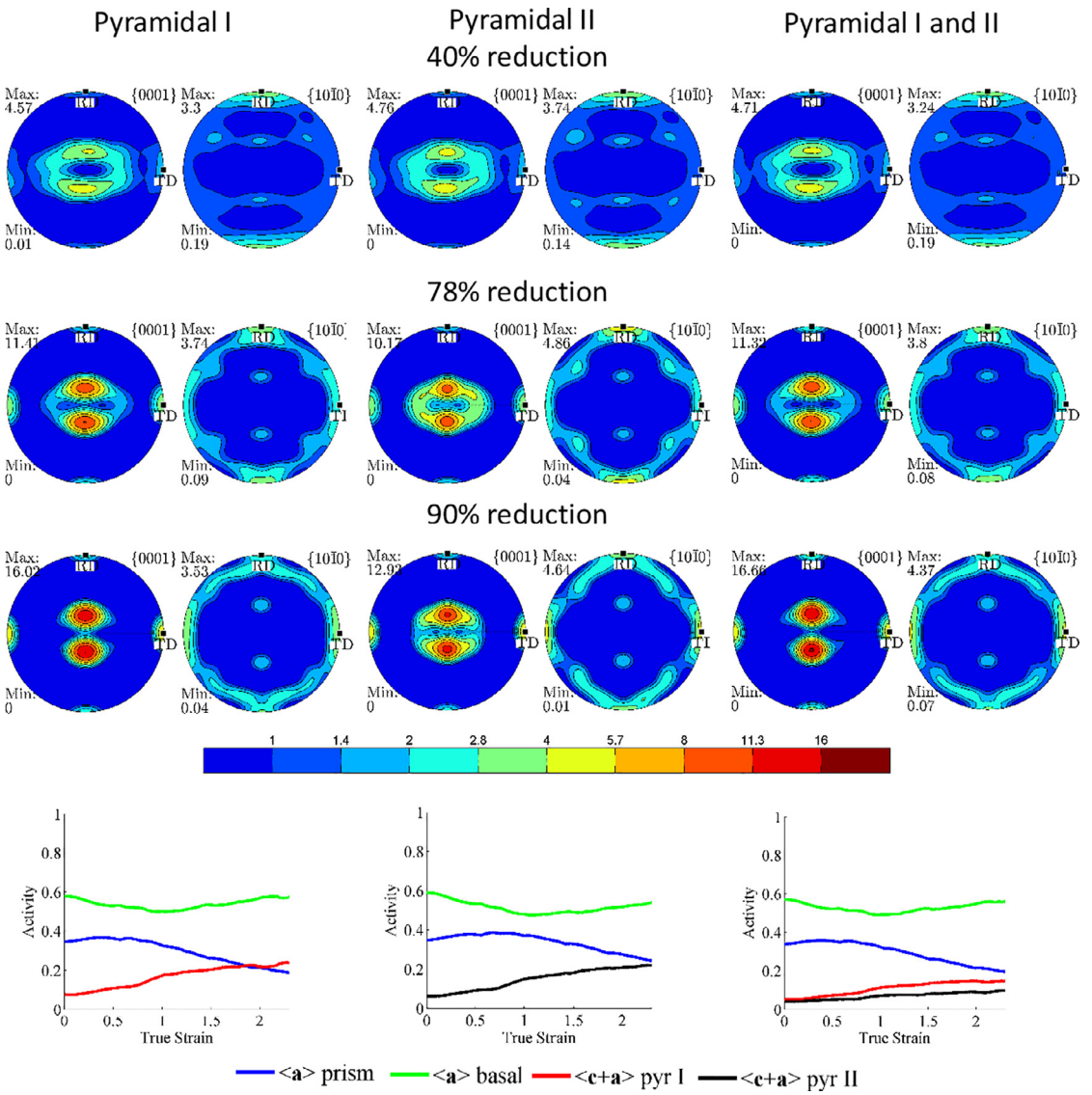

Fig. A2. Texture evolution and relative activities predicted by VPSC model at different reductions (40%, 78% and 80%) with pyramidal I or II or both I and II slip modes for a ratio of slip resistances given by: basal-prismatic-pyramidal I or II or I and II: 1-1.5-2.5. The textures were smoothed with 9° smoothing.

Supplementary materials

Supplementary material associated with this article can be found, in the online version, at doi:10.1016/j.jmps.2017.11.004.

References

Agnew, S., Yoo, M., Tome, C., 2001. Application of texture simulation to understanding mechanical behavior of Mg and solid solution alloys containing Li or Y. Acta. Mater. 49, 4277–4289.

Ando, S., Gotoh, T., Tonda, H., 2002. Molecular dynamics simulation of< c+ a>dislocation core structure in hexagonal-close-packed metals. Metall. Mater. Trans. A 33, 823–829.

Ando, S., Tonda, H., 2000. Non-basal slips in magnesium and magnesium-lithium alloy single crystals. In: Materials Science Forum. Trans Tech Publcations, pp. 43–48.

Ardeljan, M., Beyerlein, I.J., Knezevic, M., 2014. A dislocation density based crystal plasticity finite element model: application to a two-phase polycrystalline HCP/BCC composites. J. Mech. Phys. Solids 66, 16–31.

Ardeljan, M., Beyerlein, I.J., Knezevic, M., 2017. Effect of dislocation density-twin interactions on twin growth in AZ31 as revealed by explicit crystal plasticity finite element modeling. Int. J. Plast. 99, 81–101.

Ardeljan, M., Beyerlein, I.J., McWilliams, B.A., Knezevic, M., 2016a. Strain rate and temperature sensitive multi-level crystal plasticity model for large plastic deformation behavior: Application to AZ31 magnesium alloy. Int. J. Plast. 83, 90–109.

Ardeljan, M., McCabe, R.J., Beyerlein, I.J., Knezevic, M., 2015. Explicit incorporation of deformation twins into crystal plasticity finite element models. Comput. Methods Appl. Mech. Eng. 295, 396–413.

Ardeljan, M., Savage, D.J., Kumar, A., Beyerlein, I.J., Knezevic, M., 2016b. The plasticity of highly oriented nano-layered Zr/Nb composites. Acta. Mater. 115, 189–203.
Beyerlein, I.J., Lebensohn, R.A., Tomé, C.N., 2003. Modeling texture and microstructural evolution in the equal channel angular extrusion process. Mater. Sci. Eng. 345, 122–138.
Bhattacharyya, A., Knezevic, M., Abouaf, M., 2015. Characterization of crystallographic texture and intra-grain morphology in cross-rolled tantalum. Metall. Mater. Trans. A 46, 1085–1096.
Byer, C.M., Li, B., Cao, B., Ramesh, K.T., 2010. Microcompression of single-crystal magnesium. Scr. Mater. 62, 536–539.
Chelladurai, I., Miles, M.P., Fullwood, D.T., Carsley, J.E., Mishra, R.K., Beyerlein, I.J., Knezevic, M., 2017. Microstructure correlation with formability for biaxial stretching of magnesium alloy AZ31B at mildly elevated temperatures. JOM 69, 907–914.
Clausen, B., Tomé, C.N., Brown, D.W., Agnew, S.R., 2008. Reorientation and stress relaxation due to twinning: modeling and experimental characterization for Mg. Acta. Mater. 56, 2456–2468.
Fromm, B.S., Adams, B.L., Ahmadi, S., Knezevic, M., 2009. Grain size and orientation distributions: application to yielding of α-titanium. Acta. Mater. 57, 2339–2348.
Jahedi, M., McWilliams, B.A., Moy, P., Knezevic, M., 2017. Deformation twinning in rolled WE43-T5 rare earth magnesium alloy: Influence on strain hardening and texture evolution. Acta. Mater. 131, 221–232.
Jain, A., Agnew, S.R., 2007. Modeling the temperature dependent effect of twinning on the behavior of Mg alloy AZ31 sheet. Mater. Sci. Eng. A 29–36.
Jiang, L., Jonas, J.J., Mishra, R.K., Luo, A.A., Sachdev, A.K., Godet, S., 2007. Twinning and texture development in two Mg alloys subjected to loading along three different strain paths. Acta. Mater. 55, 3889.
Kabirian, F., Khan, A.S., Gnäupel-Herlod, T., 2015. Visco-plastic modeling of mechanical responses and texture evolution in extruded AZ31 magnesium alloy for various loading conditions. Int. J. Plast. 68, 1–20.
Kalidindi, S.R., Bronkhorst, C.A., Anand, L., 1992. Crystallographic texture evolution in bulk deformation processing of FCC metals. J. Mech. Phys. Solids 40, 537–569.
Kalidindi, S.R., Duvvuru, H.K., Knezevic, M., 2006. Spectral calibration of crystal plasticity models. Acta. Mater. 54, 1795–1804.
Kim, D.-H., Ebrahimi, F., Manuel, M., Tulenko, J., Phillpot, S., 2011. Grain-boundary activated pyramidal dislocations in nano-textured Mg by molecular dynamics simulation. Mater. Sci. Eng. A 528, 5411–5420.
Knezevic, M., Al-Harbi, H.F., Kalidindi, S.R., 2009. Crystal plasticity simulations using discrete fourier transforms. Acta. Mater. 57, 1777–1784.
Knezevic, M., Beyerlein, I.J., Brown, D.W., Sisneros, T.A., Tomé, C.N., 2013a. A polycrystal plasticity model for predicting mechanical response and texture evolution during strain-path changes: application to beryllium. Int. J. Plast. 49, 185–198.
Knezevic, M., Beyerlein, I.J., Lovato, M.L., Tomé, C.N., Richards, A.W., McCabe, R.J., 2014a. A strain-rate and temperature dependent constitutive model for BCC metals incorporating non-Schmid effects: application to tantalum–tungsten alloys. Int. J. Plast. 62, 93–104.
Knezevic, M., Beyerlein, I.J., Nizolek, T., Mara, N.A., Pollock, T.M., 2013b. Anomalous basal slip activity in zirconium under high-strain deformation. Mater. Res. Lett. 1, 133–140.
Knezevic, M., Bhattacharyya, A., 2017. Characterization of microstructure in Nb rods processed by rolling: effect of grooved rolling die geometry on texture uniformity. Int. J. Refract. Metals Hard Mater. 66, 44–51.
Knezevic, M., Capolungo, L., Tomé, C.N., Lebensohn, R.A., Alexander, D.J., Mihaila, B., McCabe, R.J., 2012. Anisotropic stress-strain response and microstructure evolution of textured α-uranium. Acta. Mater. 60, 702–715.
Knezevic, M., Crapps, J., Beyerlein, I.J., Coughlin, D.R., Clarke, K.D., McCabe, R.J., 2016a. Anisotropic modeling of structural components using embedded crystal plasticity constructive laws within finite elements. Int. J. Mech. Sci. 105, 227–238.
Knezevic, M., Daymond, M.R., Beyerlein, I.J., 2016b. Modeling discrete twin lamellae in a microstructural framework. Scr. Mater. 121, 84–88.
Knezevic, M., Drach, B., Ardeljan, M., Beyerlein, I.J., 2014b. Three dimensional predictions of grain scale plasticity and grain boundaries using crystal plasticity finite element models. Comput. Methods Appl. Mech. Eng. 277, 239–259.
Knezevic, M., Jahedi, M., Korkolis, Y.P., Beyerlein, I.J., 2014c. Material-based design of the extrusion of bimetallic tubes. Comput. Mater. Sci. 95, 63–73.
Knezevic, M., Kalidindi, S.R., Fullwood, D., 2008a. Computationally efficient database and spectral interpolation for fully plastic Taylor-type crystal plasticity calculations of face-centered cubic polycrystals. Int. J. Plast. 24, 1264–1276.
Knezevic, M., Kalidindi, S.R., Mishra, R.K., 2008b. Delineation of first-order closures for plastic properties requiring explicit consideration of strain hardening and crystallographic texture evolution. Int. J. Plast. 24, 327–342.
Knezevic, M., Lebensohn, R.A., Cazacu, O., Revil-Baudard, B., Proust, G., Vogel, S.C., Nixon, M.E., 2013c. Modeling bending of α-titanium with embedded polycrystal plasticity in implicit finite elements. Mater. Sci. Eng. A 564, 116–126.
Knezevic, M., Levinson, A., Harris, R., Mishra, R.K., Doherty, R.D., Kalidindi, S.R., 2010. Deformation twinning in AZ31: influence on strain hardening and texture evolution. Acta. Mater. 58, 6230–6242.
Knezevic, M., Zecevic, M., Beyerlein, I.J., Lebensohn, R.A., 2016c. A numerical procedure enabling accurate descriptions of strain rate-sensitive flow of polycrystals within crystal visco-plasticity theory. Comput. Methods Appl. Mech. Eng. 308, 468–482.
Kocks, U.F., Tomé, C.N., Wenk, H.-R., 1998. Texture and Anisotropy. Cambridge University Press, Cambridge, UK.
Kumar, A., Morrow, B.M., McCabe, R.J., Beyerlein, I.J., 2017. First-principles study of hc + ai dislocations in Mg. Mater. Sci. Eng. A (submitted).
Lebensohn, R.A., Tomé, C.N., 1993. A self-consistent anisotropic approach for the simulation of plastic deformation and texture development of polycrystals: Application to zirconium alloys. Acta Metall. Mater. 41, 2611–2624.
Lebensohn, R.A., Zecevic, M., Knezevic, M., McCabe, R.J., 2016. Average intragranular misorientation trends in polycrystalline materials predicted by a viscoplastic self-consistent approach. Acta. Mater. 104, 228–236.
Lentz, M., Klaus, M., Beyerlein, I.J., Zecevic, M., Reimers, W., Knezevic, M., 2015a. In situ X-ray diffraction and crystal plasticity modeling of the deformation behavior of extruded Mg–Li–(Al) alloys: an uncommon tension–compression asymmetry. Acta. Mater. 86, 254–268.
Lentz, M., Klaus, M., Wagner, M., Fahrenson, C., Beyerlein, I.J., Zecevic, M., Reimers, W., Knezevic, M., 2015b. Effect of age hardening on the deformation behavior of an Mg–Y–Nd alloy: In-situ X-ray diffraction and crystal plasticity modeling. Mater. Sci. Eng. A 628, 396–409.
Li, B., Ma, E., 2009. Pyramidal slip in magnesium: Dislocations and stacking fault on the {10 1 1} plane. Philosoph. Mag. 89, 1223–1235.
Li, X., Al-Samman, T., Gottstein, G., 2011. Mechanical properties and anisotropy of ME20 magnesium sheet produced by unidirectional and cross rolling. Mater. Des. 32, 4385–4393.
Nogaret, T., Curtin, W.A., Yasi, J.A., Hector Jr, L.G., Trinkle, D.R., 2010. Atomistic study of edge and screw ⟨c+a⟩ dislocations in magnesium. Acta. Mater. 58, 4332–4343.
Obara, T., Yoshinga, H., Morozumi, S., 1973. 11-22<-1-123>Slip system in magnesium. Acta Metall. 21, 845–853.
Partridge, P.G., 1967. The crystallography and deformation modes of hexagonal close-packed metals. Metallurgia 12, 169 Revised.
Reed-Hill, R., Robertson, W., 1957. Additional modes of deformation twinning in magnesium. Acta Metall. 5, 717–727.
Risse, M., Lentz, M., Fahrenson, C., Reimers, W., Knezevic, M., Beyerlein, I.J., 2017. Elevated temperature effects on the plastic anisotropy of an extruded Mg-4 Wt Pct Li alloy: experiments and polycrystal modeling. Metall. Mater. Trans. A 48, 446–458.
Risse, M.S., Lentz, M.C., Fahrenson, C., Reimers, W., Knezevic, M., Beyerlein, I.J., 2016. Elevated temperature effects on the plastic anisotropy of an extruded Mg-4wt.%Li alloy: experiments and polycrystal modeling. Metall. Mater. Trans. A..
Sachs, G., 1929. Zur Ableitung einer Fließbedingung, Mitteilungen der deutschen Materialprüfungsanstalten: Sonderheft IX: Arbeiten aus dem Kaiser Wilhelm-Institut für Metallforschung und demStaatlichen Materialprüfungsamt zu Berlin-Dahlem. Springer, Berlin Heidelberg, Berlin, Heidelberg, pp. 94–97.
Savage, D.J., Beyerlein, I.J., Knezevic, M., 2017. Coupled texture and non-Schmid effects on yield surfaces of body-centered cubic polycrystals predicted by a crystal plasticity finite element approach. Int. J. Solids Structures 109, 22–32.

Shaffer, J.B., Knezevic, M., Kalidindi, S.R., 2010. Building texture evolution networks for deformation processing of polycrystalline fcc metals using spectral approaches: applications to process design for targeted performance. Int. J. Plast. 26, 1183–1194.
Styczynski, A., Hartig, C., Bohlen, J., Letzig, D., 2004. Cold rolling textures in AZ31 wrought magnesium alloy. Scripta Mater. 50, 943–947.
Syed, B., Geng, J., Mishra, R.K., Kumar, K.S., 2012. [0 0 0 1] compression response at room temperature of single-crystal magnesium. Scr. Mater. 67, 700–703.
Tang, Y., El-Awady, J.A., 2014. Formation and slip of pyramidal dislocations in hexagonal close-packed magnesium single crystals. Acta. Mater. 71, 319–332.
Taylor, G.I., 1938. Plastic strain in metals. J. Inst. Metals 62, 307–324.
Tomé, C., Necker, C., Lebensohn, R., 2002. Mechanical anisotropy and grain interaction in recrystallized aluminum. Metall. Mater. Trans. A 33, 2635–2648.
Tonda, H., Ando, S., 2002. Effect of temperature and shear direction on yield stress by 11-22 <-1-123>slip in HCP metalsslip in HCP metals. Metall. Mater. Trans. A 33, 831–836.
Turner, P.A., Tomé, C.N., 1994. A study of residual stresses in Zircaloy-2 with rod texture. Acta Metall. Mater. 42, 4143–4153.
Wang, Y.N., Huang, J.C., 2003. Texture analysis in hexagonal materials. Mater. Chem. Phys. 81, 11–26.
Wu, Z., Curtin, W., 2015. The origins of high hardening and low ductility in magnesium. Nature 526, 62–67.
Wu, Z., Curtin, W.A., 2016. Intrinsic structural transitions of the pyramidal I $\langle c+a \rangle$ dislocation in magnesium. Scr. Mater. 116, 104–107.
Wu, Z., Francis, M., Curtin, W., 2015. Magnesium interatomic potential for simulating plasticity and fracture phenomena. Modell. Simul. Mater. Sci. Eng. 23, 015004.
Xie, K.Y., Alam, Z., Caffee, A., Hemker, K.J., 2016. Pyramidal I slip in c-axis compressed Mg single crystals. Scr. Mater. 112, 75–78.
Yoo, M.H., 1981. Slip, twinning, and fracture in hexagonal close-packed metals. Metall. Mater. Trans. A 12, 409–418.
Yu, Q., Qi, L., Mishra, R.K., Li, J., Minor, A.M., 2013. Reducing deformation anisotropy to achieve ultrahigh strength and ductility in Mg at the nanoscale. Proc. National Acad. Sci. 110, 13289–13293.
Zecevic, M., Beyerlein, I.J., Knezevic, M., 2017a. Coupling elasto-plastic self-consistent crystal plasticity and implicit finite elements: Applications to compression, cyclic tension-compression, and bending to large strains. Int. J. Plast. 93, 187–211.
Zecevic, M., Knezevic, M., 2015. A dislocation density based elasto-plastic self-consistent model for the prediction of cyclic deformation: Application to Al6022-T4. Int. J. Plast. 72, 200–217.
Zecevic, M., Knezevic, M., Beyerlein, I.J., McCabe, R.J., 2016a. Origin of texture development in orthorhombic uranium. Mater. Sci. Eng. A 665, 108–124.
Zecevic, M., Knezevic, M., Beyerlein, I.J., McCabe, R.J., 2016b. Texture formation in orthorhombic alpha-uranium under simple compression and rolling to high strains. J. Nuclear Mater. 473, 143–156.
Zecevic, M., Knezevic, M., Beyerlein, I.J., Tomé, C.N., 2015a. An elasto-plastic self-consistent model with hardening based on dislocation density, twinning and de-twinning: Application to strain path changes in HCP metals. Mater. Sci. Eng. A 638, 262–274.
Zecevic, M., Korkolis, Y.P., Kuwabara, T., Knezevic, M., 2016c. Dual-phase steel sheets under cyclic tension–compression to large strains: Experiments and crystal plasticity modeling. J. Mech. Phys. Solids 96, 65–87.
Zecevic, M., McCabe, R.J., Knezevic, M., 2015b. A new implementation of the spectral crystal plasticity framework in implicit finite elements. Mech. Mater. 84, 114–126.
Zecevic, M., McCabe, R.J., Knezevic, M., 2015c. Spectral database solutions to elasto-viscoplasticity within finite elements: application to a cobalt-based FCC superalloy. Int. J. Plast. 70, 151–165.
Zecevic, M., Pantleon, W., Lebensohn, R.A., McCabe, R.J., Knezevic, M., 2017b. Predicting intragranular misorientation distributions in polycrystalline metals using the viscoplastic self-consistent formulation. Acta. Mater. 140, 398–410.